Ninth International Conference on Advances in Steel Structures (ICASS'2018)
5-7 December 2018 - Hong Kong, China

ON THE NUMERICAL SIMULATION OF THE RESPONSE OF GAS PIPELINES UNDER COMPRESSION

Grigorios Tsinidis [1], Luigi Di Sarno [2]*, Anastasios Sextos [3], Nikolaos Psyrras [4] and Peter Furtner [5]

[1] University of Sannio, Benevento, Italy
E-mails: tsinidis.grigorios@gmail.com

[2] University of Sannio, Benevento, Italy & University of Liverpool, Liverpool, United Kingdom
E-mail: ldisarno@unisannio.it – luigi.di-sarno@liverpool.ac.uk

[3] University of Bristol, Bristol, United Kingdom & Aristotle University of Thessaloniki, Thessaloniki, Greece
E-mail: a.sextos@bristol.ac.uk

[4] University of Bristol, Bristol, United Kingdom
E-mail: n.psyrras@bristol.ac.uk

[5] Vienna Consulting Engineers, Vienna, Austria
E-mail: furtner@vce.at

Abstract: *Steel gas pipelines may be subjected to buckling failure under large compressive straining, caused by seismically induced ground deformations. This paper further elaborates on the buckling response of this type of networks, through the presentation of representative results from a series of axial compression static analyses that were conducted on segments of steel gas pipelines. Above ground and embedded segments of diverse radius to thickness ratios (R/t) were simulated by means of inelastic shell elements. The trench of embedded pipelines was modelled using solid elastic elements, while an advanced contact model was used to simulate the pipe-soil interface. Salient parameters that affect the axial response, including the internal pressure and the existence of imperfections on the segment, were considered in this study. In line with previous evidence, the results reveal a reduction of the axial response of the pipe segment with increasing levels of internal pressure. In parallel, internal pressure leads the limit stresses to occur at progressively higher axial deformations, while limit loads computed for embedded pipelines are higher compared to those predicted for equivalent above ground pipelines, as a result of the soil confinement.*

Keywords: Gas pipelines; Above ground pipelines; Embedded pipelines; Critical loading; imperfections

DOI: 10.18057/ICASS2018.201

1 INTRODUCTION

Natural gas pipeline networks constitute a critical means of energy transportation, playing a vital role in the economic development of modern societies. The associated socio-economic and environmental impact in case of seismically induced damages highlights the importance of a rational assessment of the seismic structural integrity of these networks.

Post-earthquake observations have demonstrated that gas pipelines may undergo extensive damage due to seismically induced permanent and transient ground movements [1]. Excessive ground movements may cause large compression loadings on pipelines, potentially leading to

shell-mode or beam buckling failures [2]. Shell-mode or local buckling is associated with the loss of stability caused by compressive or bending loading on the pipeline. For the typical radio to thickness ratios and steel grades used in NG pipeline networks, shell mode instabilities are expected in the inelastic range of response, with wrinkles beginning to develop and localize, followed by limit load instability or a secondary, usually non-axisymmetric, bifurcation. The highly localized deformations may lead to wall tearing and hence content leakage. Beam or upheaval buckling, which is likely to occur in cases of shallow small-diameter pipelines, resembles the Euler buckling mode of column, when subjected to compressive loading. This damage mode rarely leads to breakage; however, it may reduce the flow of content, thus affecting serviceability.

The paper aims to further elaborate on the buckling response of gas pipelines under compressive loading that may be caused by seismically induced ground deformations particularly in the case of abruptly changing soil profiles along the pipeline length. A series of compression static analyses, which were carried out on above ground and embedded segments of steel pipelines, are presented, examining salient parameters that control the axial compression response of this type of structures. The presented results highlight the differences on the axial response of above ground and embedded gas pipelines under axial compression loading. In parallel, insights on critical simulation aspects are provided, which may contribute towards the development of more efficient numerical models for the seismic design and structural assessment of gas pipelines.

2 CASE STUDIES AND NUMERICAL SIMULATION

2.1 Case studies

Six pipe segments made of API X65 steel were studied, covering a wide range of diameters and radius to thickness (R/t) ratios that are commonly found in gas pipeline networks. Table 1 summarizes the geometric and material properties of the selected cases. The length of the examined segments was set equal to five times their diameter. The segments were examined as part of either above ground or embedded pipelines. In the latter cases, the burial depth to the pipeline crown was set equal to 1.0 m, with the surrounding ground - trench simply constraining the pipeline in the normal direction of the pipe-soil interface.

Table 1: Geometric and material properties of the examined pipeline segments.

Diameter (in)	Diameter (cm)	Thickness (mm)	R/t ratio	Yield stress σ_y (MPa)	Ultimate strain ε_u (%)
16	406.4	10.3	19.7	448	4
24	609.6	9.5	32.1	448	4
30	762	17.5	21.8	448	4
36	914.4	12.7	36.0	448	4
42	1066.8	19.1	27.9	448	4
48	1219.2	23.8	25.6	448	4

2.2 Numerical simulation

A series of compression static analyses were carried out on the selected pipe segments, using the general-purpose finite element code ABAQUS [3]. The axial response of the segments under compression was reported through a modified Riks solution algorithm. Figures 1a and 1b, illustrate the typical numerical models of an above ground and the equivalent embedded pipe segment, respectively.

The pipe segments were simulated as thin cylindrical shell models, following the Koiter-Sanders theory. Inelastic, reduced integration S4R shell elements were used for the discretization of the models, having both membrane and bending stiffness. The mesh density

was selected, so as to resolve the elastic buckling modes of the examined segments, assuming these as unconstrained axially compressed cylindrical shells. Along these lines, a series of buckling eigenvalue analyses were conducted for various mesh densities. Accounting for the elastic modulus E = 200 GPa and the Poisson's ratio v = 0.3 of the steel grade adopted herein, the theoretical axial half-wavelength was defined as $\lambda_c \approx 1.72\sqrt{Rt}$ [4]. Element lengths, ranging between 2.0 cm and 4.0 cm, were found capable to reproduce the theoretical axial half-wavelength λ_c of the examined segments. The plastic behavior of steel was modelled through a classical flow plasticity model combined with a von Mises yield criterion. In particular, a Ramberg-Osgood curve (yield offset equal to 0.5%, hardening exponent n = 12), was fitted to a bilinear isotropic curve, with the latter describing the tensile uniaxial behaviour of the selected steel grade (Figure 1c).

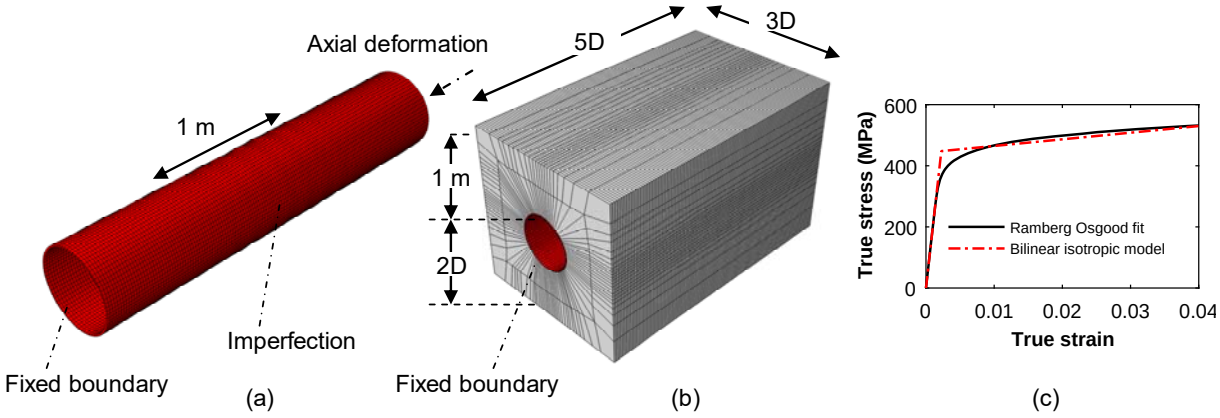

Figure 1: Representative numerical models of (a) above ground and (b) embedded pipe segment (D = 914.4 mm), (c) uniaxial tensile stress-strain response of API X65 steel (n = 12, α = yield offset × E/σ_y)

Both 'perfect' segments and segments with geometry perturbation were considered, so as to investigate the effect of pipe imperfections on the axial response. For the latter cases, a stress-free, biased axisymmetric imperfection was considered at a short zone of 1.0 m, which was set at the middle of the segment. The imperfection was defined on the basis of a sinusoid modulated by a second sinusoid, thus resulting in a peak amplitude at the middle section of the segment [5]:

$$\bar{w}(x) = \left[w_0 + w_1 \cos\left(\frac{\pi x}{N\lambda_c} \right) \right] \cos\left(\frac{\pi x}{\lambda_c} \right), \quad -\frac{L_{crit}}{2} \le x \le \frac{L_{crit}}{2}, \quad L_{crit} = 1.0m, \quad 2N\lambda_c = L_{crit} \tag{1}$$

The peak amplitude of the imperfection was set as a function of the pipe lining thickness, based on the following formulation: $w = w_0 + w_1 = 0.10t$. Additional analyses were conducted for selected cases, doubling the imperfection amplitude, i.e. $w = w_0 + w_1 = 0.20t$.

The soil trench, surrounding the embedded segments, was simulated by means of reduced-integration linear elastic solid elements (i.e. C3D8R elements). The meshing of soil trench was selected on the basis of a preliminary sensitivity analysis, which indicated that more a refined model had a negligible effect on the computed pipe response, increasing significantly the computational cost. The distance between the side boundaries of the trench model and the pipe edges was set equal to one pipe diameter (Figure 1b). A similar distance was adopted between the pipe invert and the bottom boundary of the trench model, while the distance between the surface of the soil-trench and the crown of the pipe was set equal to 1.0 m. The soil mechanical properties were selected, so as to correspond to a dense sand material, which is commonly used in practice. In particular, the following properties were adopted: density ρ

= 1.8 t/m^3, shear modulus G = 23.4 MPa, Poisson's ratio, v = 0.33. Additional analyses were carried out in the framework of a sensitivity study, doubling the trench shear stiffness. The mesh density along the longitudinal axis of the soil model (i.e. parallel to pipeline axis) matched exactly the pipe mesh, in order to prevent initial gaps during the generation of the perturbed mesh [6].

The pipe-soil interface was simulated by means of an advanced hard contact interaction model, available in ABAQUS [3]. The model allows the potential detachment and/or sliding between the interacting elements during loading. The shear behaviour of the interface model was controlled by the classical Coulomb friction model, through the introduction of a friction coefficient, μ. The latter was set equal to 0.3 [7].

To investigate the effect of the level of internal pressure on the axial compressive response, the analyses were conducted by assuming either non-pressurized segments (i.e. p = 0 kPa), or pressurized segments at maximum operating pressure p_{max}, the latter defined as: $p = 0.72 \times \left(2\sigma_y t/D\right)$, where σ_y is the yield stress (equal to 448 MPa herein) and D is the diameter of selected segment. Additional analyses were carried out for selected cases under intermediate pressure levels, i.e. 4 MPa (40 barr) and 8 MPa (80 barr). It is noted that other potential effects, associated with the flow of gas in the pipeline segments, e.g. straining due to temperature changes, were neglected in the present study.

The analyses were carried out in steps; initially, the internal pressure, when considered, was applied on the pipeline segment within a static step. For the embedded segments, the gravity load was also introduced within this static step, in order to introduce the in-situ stress state on the soil model and ensure the proper activation of the interface. A large-deformation static Riks step was followed, with the pipeline being fixed at one end and compressed at the opposite end in a displacement-driven fashion. The selection of displacement-driven compression analyses was made due to the computational efficiency of this approach compared to force-driven analyses, particularly at the near buckling- and the post-buckling loading regime. Forced-driven compression analyses were also conducted in the framework of a sensitivity analysis, as discussed in the ensuing. Standard static boundary conditions were applied at the boundaries of the soil model of embedded segments, which were activated throughout the analysis. The response of the examined models was reported in terms of deformation patterns, strains and stresses of the pipeline systems, as well as axial force-deformation relations. The latter were presented in normalized forms. In particular, the axial loading was normalized by the following quantity: $P_o = 2\pi Rt\sigma_y$ [8], i.e. the yield axial load of the section, and plotted against the average axial shortening δ_x/l.

3 RESULTS & DISCUSSION

3.1 Deformation patterns

During axial compression loading the examined segments are subjected to plastic buckling, which results in a drop of their axial stiffness and a significant increase of axial deformations. Contrary to elastic shell buckling, where the collapse is sudden, in plastic buckling the failure is separated from the first instability [5]. The results of the analyses presented herein verify such a response. In particular, the segments are initially deformed uniformly. At some strain level an axisymmetric deformation mode is developed in the form of wall wrinkling. With increasing compression loading the stiffness gradually drops and wrinkles grow. Parameters such as initial geometric imperfections, level of internal pressure and confinement from surrounding ground (i.e. for embedded segments), affect the location and characteristics of this wall wrinkling response, as well as the average axial force-displacement path.

Figure 2 illustrates deformed shapes of pressurized ($p = 0.72 \times p_{max}$) pipe segments with D = 609.4 mm, predicted by the numerical analyses after critical loading. Contour diagrams of the equivalent plastic strain, corresponding at this loading step, are displayed on the deformed shapes. For the perfect, above ground segment, wrinkling is developed near the end sides (Figure 2a). On the contrary, for the imperfect above ground segment, the wall wrinkling is developed at the area of initial geometric imperfection (Figure 2b). For the perfect embedded segment, the wrinkling is localized at the end side, where the axial compression loading is introduced (Figure 2c). The consideration of the geometric imperfection on the embedded pipe segment, results again in wall wrinkling at the area of geometric imperfection. It is worth noticing that the location of wrinkling is different compared to the one predicted for the equivalent above ground imperfect segment, as a result of the external confinement that is being offered by the soil-trench on the embedded segment.

Figure 3 further elaborates on the effect of soil-trench confinement on the axial deformation patterns of embedded pipes, presenting deformed shapes of pressurized ($p = 0.72 \times p_{max}$) embedded segments with D = 914.4 mm. For the perfect segment (Figure 3a), significant axial deformations are localized near the end side of the pipe, where the loading is introduced, while the opposite end experiences negligible straining. On the contrary, the equivalent pipe segment with the geometric imperfection, experiences buckling near the middle section (Figure 3b). The 'right' side of the segment slides along the pipe-soil interface after critical loading is reached, with the wrinkle increasing at the middle section, while the 'left' side of the pipe experiences low axial straining.

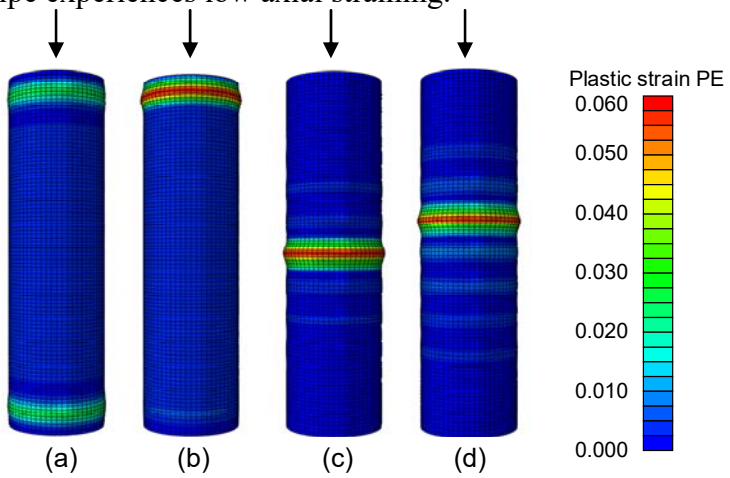

Figure 2: Contour diagrams of equivalent plastic strains on deformed shapes of pressurized pipe segments (D = 609.4 mm), predicted after critical loading; (a) perfect, above ground segment, (b) perfect, embedded segment, (c) above ground segment with imperfections (w/t = 0.1), (d) embedded segment with imperfections (w/t = 0.1)

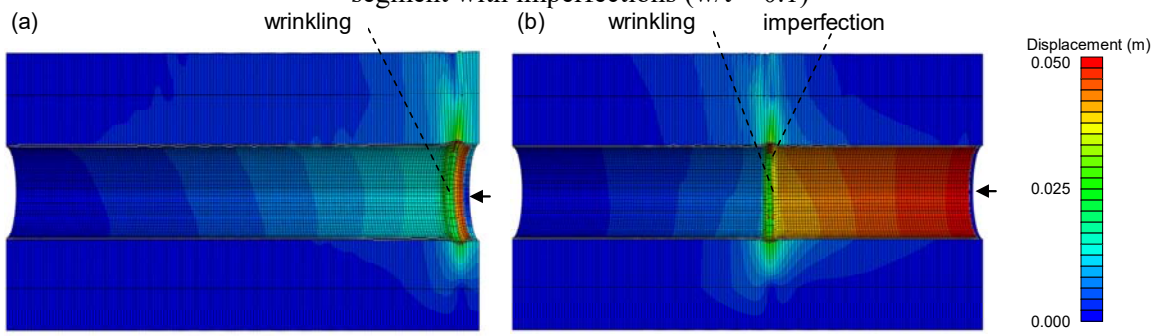

Figure 3: Contour diagrams of resultant displacement on deformed shapes of systems of trench-embedded pipe segments (D = 914.4 mm), computed after critical loading; (a) perfect segment, (b) segment with imperfection (w/t = 0.1)

3.2 Displacement-driven versus forced-driven compression analyses

Force-driven compression analyses were carried out on selected pipe segments, aiming at identifying the potential effect of simulation of 'compression loading' on the computed axial response. The analyses were conducted using the same numerical models and making the exact same assumptions, regarding all the other parameters involved. Figure 4 compares average axial force-displacement paths, predicted by displacement- and forced-driven compression analyses on above ground segments with D = 914.4 mm. The comparisons are presented for both non-pressurized and pressurized segments, either assuming or neglecting initial geometric imperfections. For all the examined cases, the relevant axial force-displacement relations are almost identical, with both analysis procedures predicting indistinguishable critical loadings for the segments. Similar conclusions were drawn for other pipe segments with diverse diameters and R/t ratios.

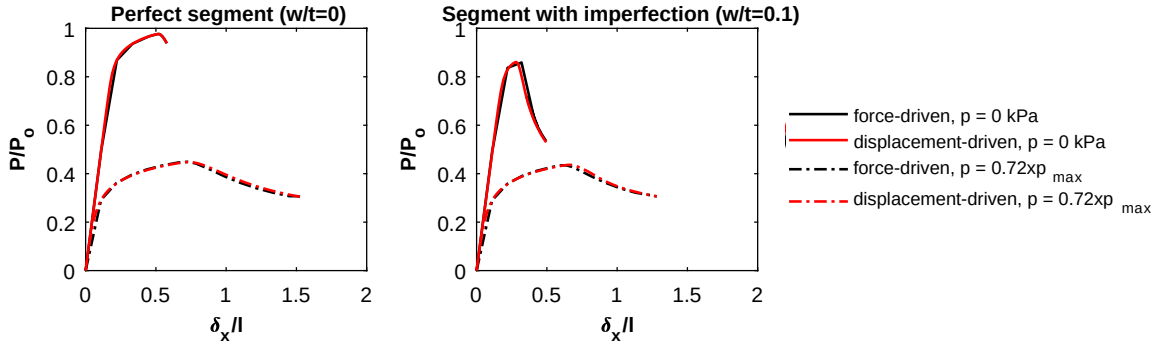

Figure 4: Average axial load-deformation paths of D = 914.4 mm above ground pipe segments, predicted by force-driven and displacement- driven compression analyses

3.3 Effect of internal pressure on the axial response

This section examines the effect of internal pressure on the axial response of gas pipelines under compression loading. For this purpose, a series of average axial load-deformation paths, predicted by compression analyses of the examined pipe segments under various levels of internal pressure, are compared. Figure 5 compares average axial load-deformation paths computed for above ground pipe segments. The dashed lines correspond to the responses of perfect segments, whereas solid lines stand for the responses of pipe segments with initial geometric imperfections. In the latter cases, the maximum amplitude of geometric imperfection is set as w/t = 0.1. It is well known that the existence of geometric imperfections on the segments result in a reduction of the axial response, compared to the one of the equivalent perfect segment. This observation is verified in the herein analyses, as well. The critical loadings of imperfect segments, as well as the axial shortening δ_x/l levels, where these loadings are observed (i.e. 'critical' axial shortening levels), are lower compared to those predicted for the equivalent perfect segments. The differences on the computed paths of perfect and equivalent imperfect segments are generally higher for non-pressurized segments, while they decrease significantly with the increase of internal pressure. Actually, for pressurized pipe segments with the maximum operation pressure (i.e. p = 0.72 p_{max}) the differences on the loading-deformation paths of equivalent perfect and imperfect segments are negligible for $\delta_x/l \prec 0.5-0.8$ (depending on the R/t ratio of the examined segment). Additionally, the consideration of internal pressure results in a general lowering of the axial load-displacement path. In parallel, the internal pressure leads the limit loading to occur at progressively higher axial shortening levels. This response, which has been verified experimentally by Paquette & Kyriakides [8], is attributed to the plastic interaction of the two loading conditions (i.e. internal pressure and axial compression), acting on the segment.

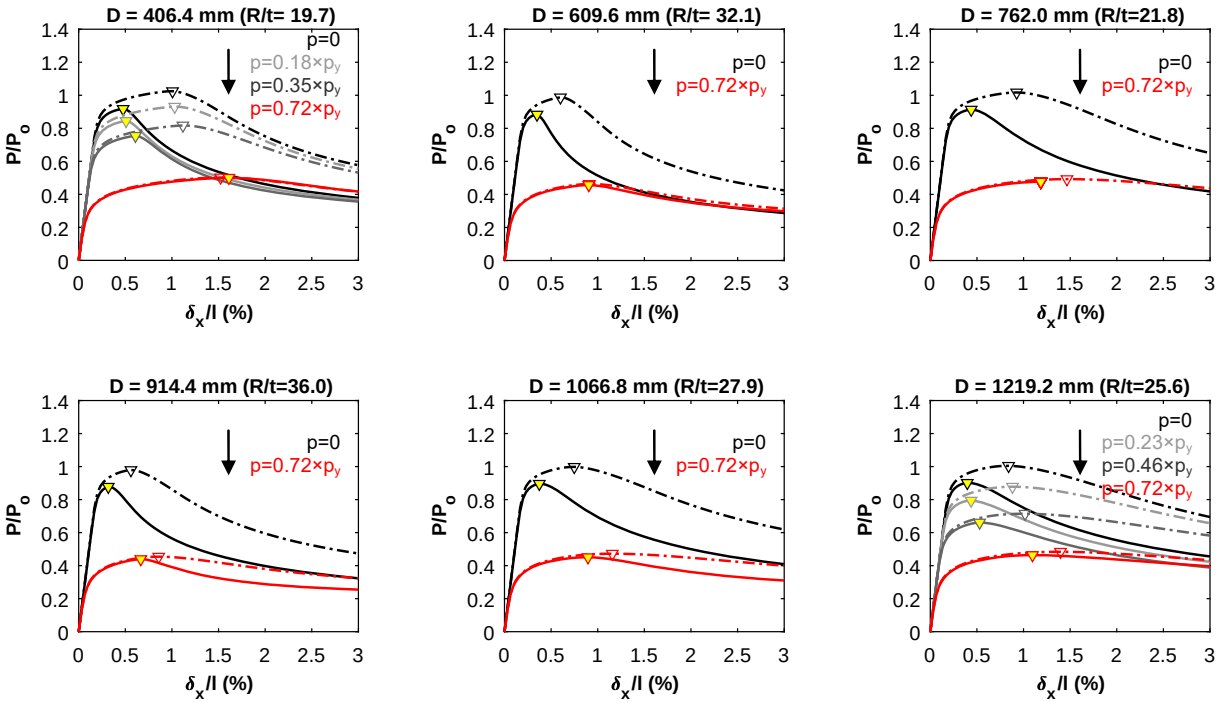

Figure 5: Average axial load- deformation paths of above ground pipe segments, computed for various levels of internal pressure; dashed lines: perfect segments, solid lines: segments with initial geometric imperfection (w/t =0.1)

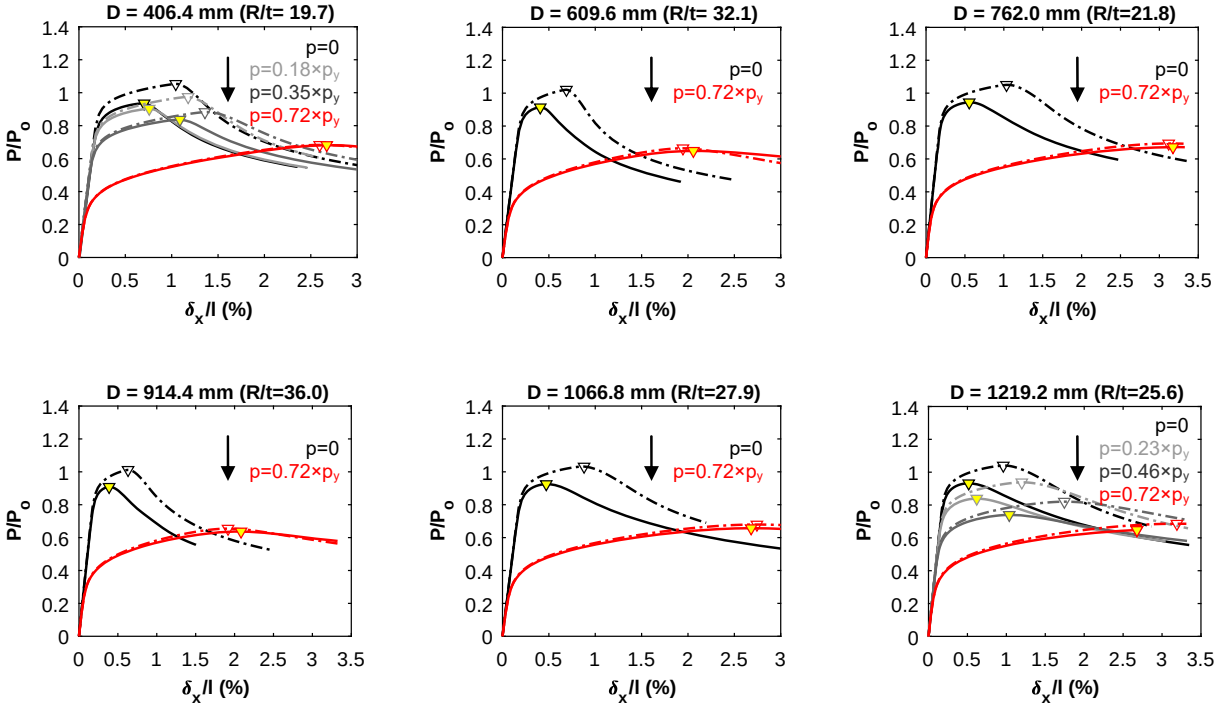

Figure 6: Average axial load- deformation paths of embedded pipe segments, computed for various levels of internal pressure; dashed lines: perfect segments, solid lines: segments with initial geometric imperfection (w/t =0.1)

Figure 6 portrays similar comparisons of axial load-deformation paths, referring to embedded pipe segments. The comparisons are again provided for various levels of internal pressure. Similar to the above ground segments, the dashed lines correspond to the paths computed for perfect segments, whereas solid lines stand for segments with geometric

imperfections (w/t = 0.1). Generally, the confinement, which is offered by the soil-trench, 'stabilizes' the axial response of embedded segments, leading to an increase of the axial load-deformation response compared to the one of the equivalent above ground segments (i.e. higher critical loadings and 'critical' shortening levels are identified for embedded segments compared to the ones of the equivalent above ground segments). The consideration of the geometric imperfections reduces the axial response of pipelines compared to the perfect segments. However, the differences between the axial response of perfect and imperfect segments are smaller compared to those revealed for above ground segments, particularly for higher levels of internal pressure. In line with the response of above ground pipe segments, the increase of internal pressure leads to a general reduction of the axial load-deformation paths and a general increase of the 'critical' axial shortening levels where buckling occurs.

3.4 Effect of geometric imperfection amplitude on the axial response

The effect of the amplitude of initial geometric imperfection on the axial response of the examined segments is presented in this section. Figure 7 compares average axial force-deformation paths computed for different above ground segments under various levels of geometric imperfections amplitudes. The comparisons are plotted for both non-pressurized and pressurized segments. The axial response of the segments reduces with increasing imperfection amplitude (i.e. lower responses are reported for w/t = 0.2). This is generally more evident in case of non-pressurized segments (i.e. p = 0) and for segments with lower R/t ratios. The pressurization of the segments reduces the detrimental effect of initial geometric imperfections.

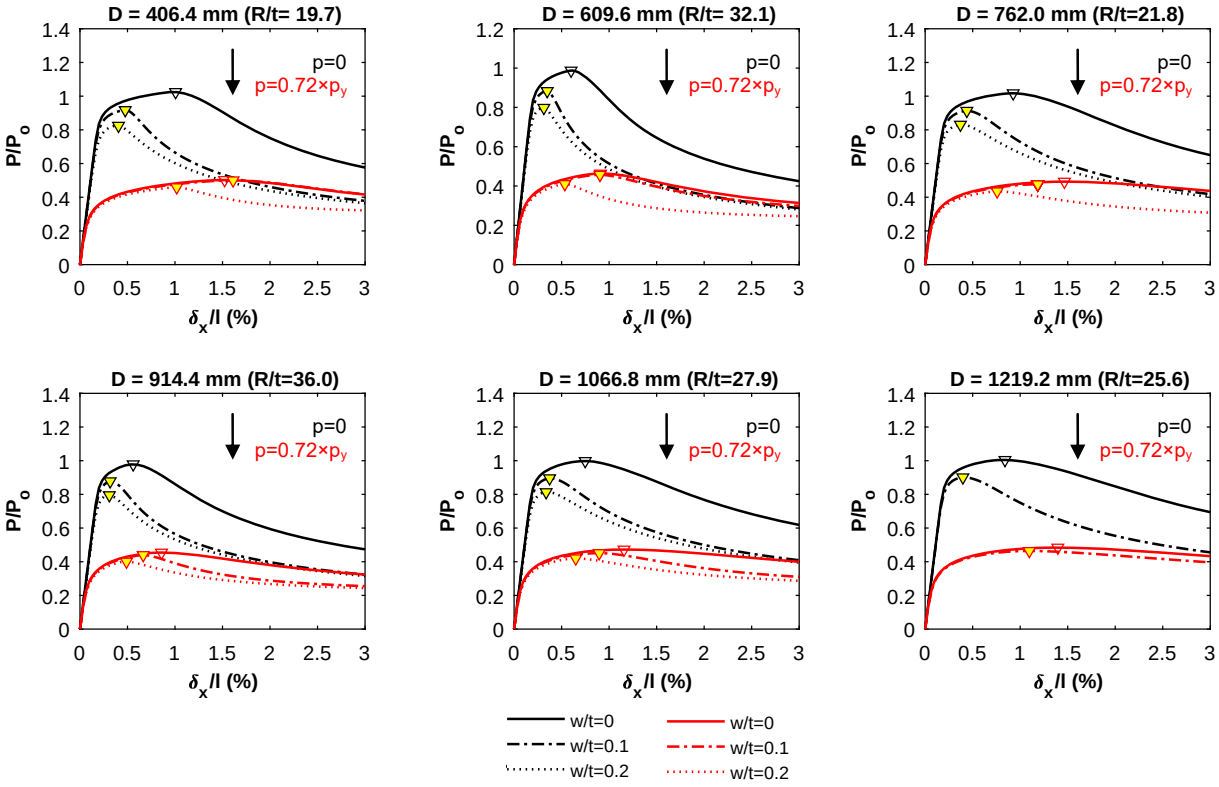

Figure 7: Average axial load-deformations paths of above ground pipe segments, computed for various amplitudes of initial geometric imperfections

The effect of imperfection amplitude on the axial force-deformation paths of the examined embedded pipe segments is presented in Figure 8. The confinement that is offered by the

surrounding ground (i.e. trench) reduces the effect of imperfection on the axial response of the examined segments, particularly for the cases of pressurized segments. Actually, for the pressurized segments with the maximum operational pressure level (p = 0.72 p_{max}), the axial force-deformation paths predicted by the analyses of equivalent perfect and imperfect segments are quite similar, even in the post-buckling regime.

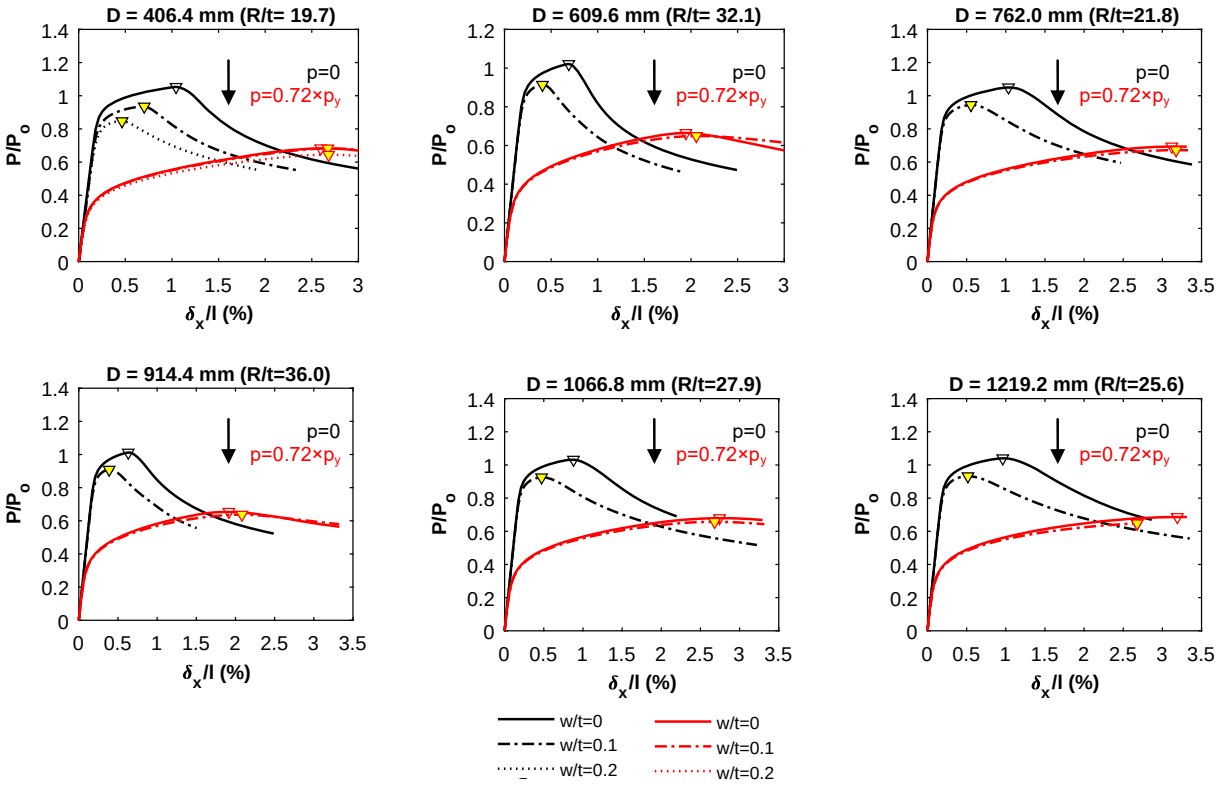

Figure 8: Average axial load-deformations paths of embedded pipe segments, computed for various amplitudes of initial geometric imperfections

3.5 Effect of radius to thickness ratio (R/t) on the axial response

Figure 9 highlights the effect of R/t ratio on the average axial force-deformation paths, predicted for representative segments. Generally, the axial response of the segments reduces with the increase of the R/t ratio. This observation is evident for either pressurized or non-pressurized, above ground or embedded segments, regardless of the existence of initial geometric imperfections.

To further elaborate on the effect of R/t ratio of the pipe segment on its axial response, the computed 'critical' average axial shortening δ_x/l levels (i.e. the average axial shortening levels that correspond to critical loading) and the critical stresses of examined segments are plotted against the relevant R/t ratios in Figure 10. The critical stresses and the 'critical' axial shortening levels are both decreasing with increasing R/t ratio. Higher critical stresses and 'critical' axial shortening levels are predicted for embedded pipe segments, while the consideration of initial geometric imperfections result in a decrease of both response characteristics. The higher the amplitude of the initial imperfection, the higher the differences between the above response characteristics of equivalent perfect and imperfect segments are.

In line with the previous results and discussion, the critical loadings of pressurized segments are reported at higher levels of axial shortening δ_x/l, compared to the non-pressurized segments. Indeed, the 'critical' axial shortening level of non-pressurized segments can be as high as 1.05 % for the examined perfect embedded segments, whereas for the

equivalent pressurized segments the critical axial shortening level increases up to 2.6-2.7 %. On the contrary, the critical stress of pressurized pipe segments is reduced compared to the one predicted for the equivalent non-pressurized segments. It is worth noticing the reduced differences between the critical stresses of perfect and imperfect embedded segments, when a significant internal pressure is considered (i.e. p = 0.75 p_{max} in Figure 10d).

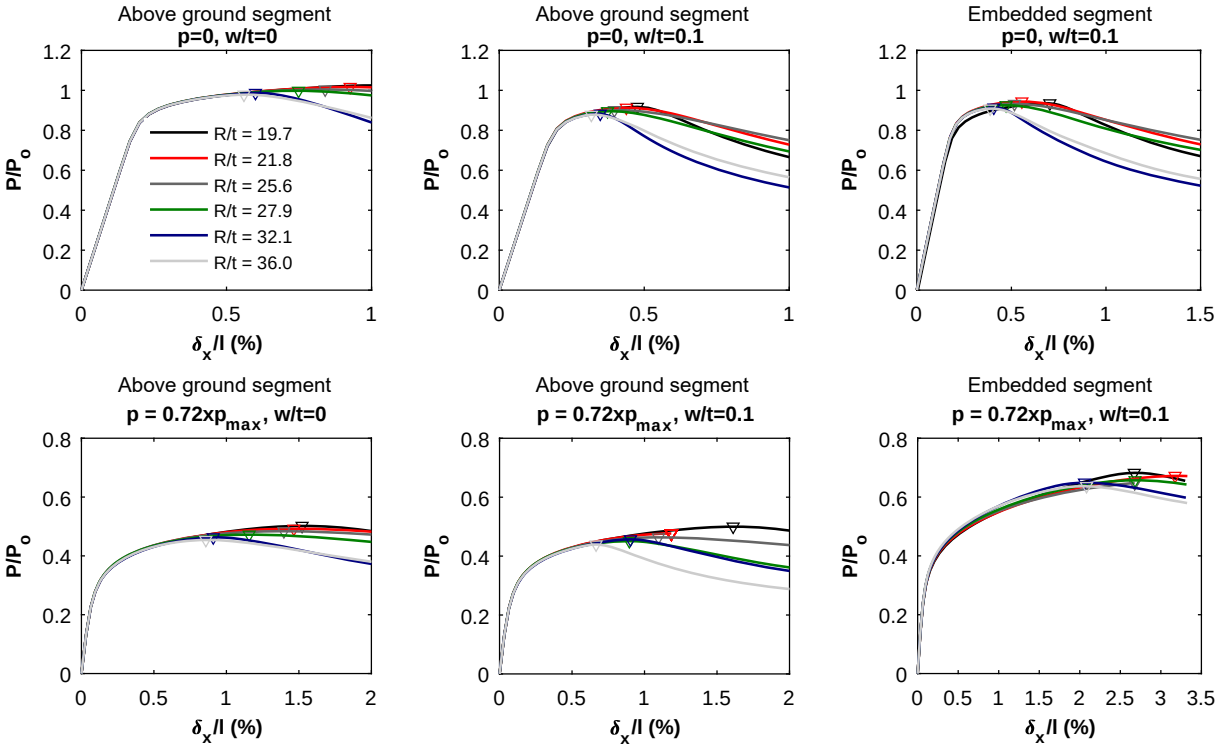

Figure 9: Effect of R/t ratio on the average axial load-deformation paths of above ground and embedded pipe segments, computed by either considering or neglecting initial geometric imperfections

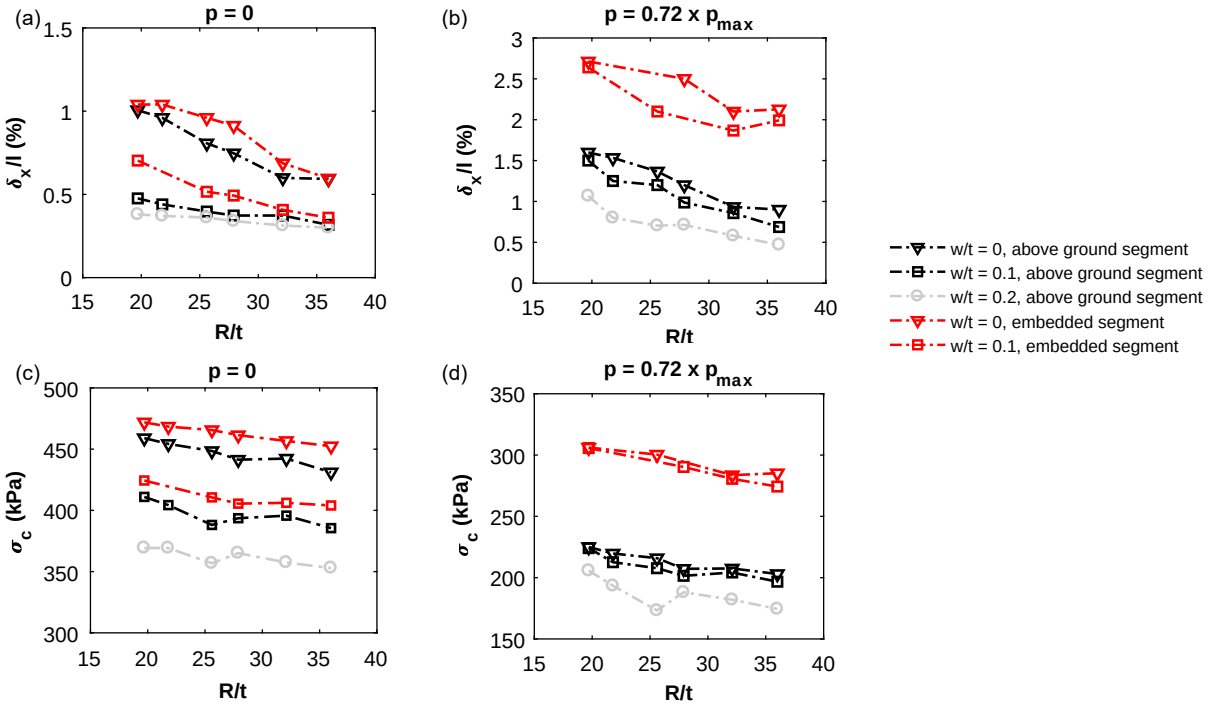

Figure 10: Effect of R/t ratio on the 'critical' average axial shortening δ_x/l of (a) non-pressurized and (b) pressurized segments and the critical stress of (c) non-pressurized and (b) pressurized segments

3.6 Effect of soil-trench stiffness on the axial response of embedded pipe segments

In the discussion made so far, the trench stiffness was fixed to a certain level. To investigate the effect of this parameter on the axial compression response of embedded pipes, additional analyses were conducted on selected embedded segments (i.e. D = 1066.8 and 1219.2 mm), doubling the stiffness of the soil-trench. Figure 11 compares the computed axial force-deformation paths for these cases. The comparisons are provided for both non-pressurized and pressurized segments, either considering or neglecting the initial geometric imperfections. Solid lines correspond to the results referring to the initial soil-trench stiffness, while dashed lines stand for the analyses, where increased soil stiffness is considered. As theoretically expected, the increase of soil stiffness, results in an increasing stabilization of the segment, which in turn results in an increase of its axial response. This is more evident for the non-pressurized pipe segment.

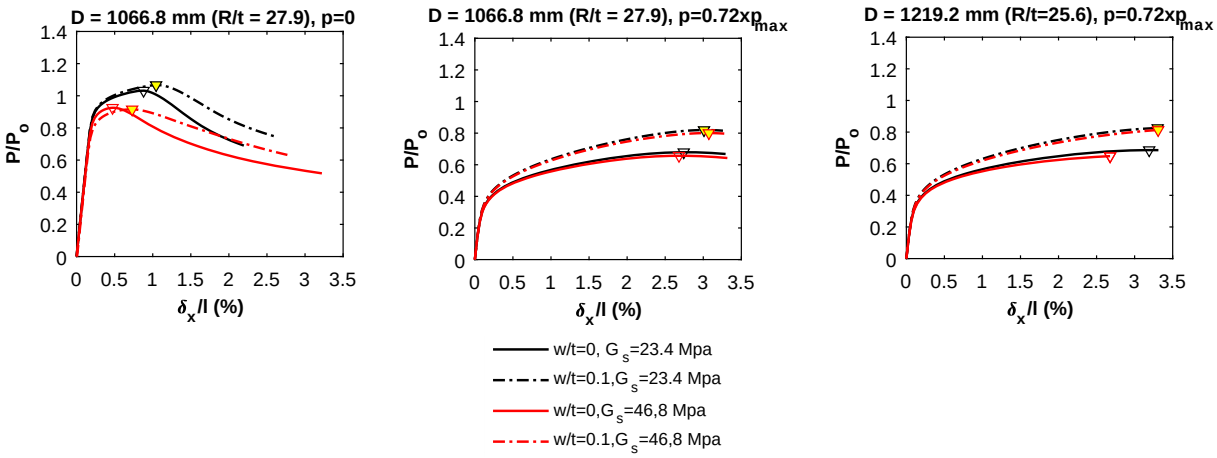

Figure 11: Effect of the stiffness of the soil-trench on the average axial load-deformation paths computed on non-pressurized or pressurized segments, when considering or neglecting the initial geometric imperfections

4 CONCLUSIONS

The paper discussed representative results of a series of compression static analyses that were conducted to further elaborate on crucial parameters affecting the buckling response of gas pipelines under large compressive loading that may occur due to propagation of seismic waves within inhomogeneous soil media, particularly for the case of abruptly changing soil conditions. Both above ground and embedded segments of steel pipelines with diverse radius to thickness (R/t) ratios were analyzed, considering different parameters that might affect the axial response. The key findings of this study are summarized below:

- Forced- and displacement-driven compression analyses of pipe segments resulted in similar axial force-deformation paths. The latter were selected in this study, since they found more efficient computationally, particularly in the near and post-buckling regime.
- Under increasing axial compression loading the segments were initially axially deformed; at some strain level an axisymmetric deformation mode was developed in the form of wall wrinkling. With increasing compression loading the stiffness gradually dropped and the wrinkles grew.
- The existence of initial geometric imperfections, the level of internal pressure, as well as the confinement from surrounding ground (i.e. trench for embedded segments), affected

the location and characteristics of this wall wrinkling response, as well as the average axial force-displacement path.

- The analyses revealed a reduction of the axial response with increasing levels of internal pressure for both above ground and embedded pipelines, with the reduction being more pronounced in the former case.
- Internal pressure led the limit stresses to occur at progressively higher strains, while limit loads computed for embedded pipelines were generally higher compared to those predicted for similar above ground pipelines.
- The increase of the trench stiffness led in an enhancement of its axial response. This was particularly evident for non-pressurized pipe segments.

Along these lines, the examined parameters, i.e. the internal pressure, the initial geometric imperfections and the mechanical and physical properties of the trench, should be adequately accounted for in relevant studies. Further research is currently pursued towards the development of more efficient numerical models for the seismic design and structural assessment of gas pipelines, accounting for the above salient parameters.

5 ACKNOWLEDGMENTS

This work was supported by the Horizon 2020 Programme of the European Commission under the MSCA-RISE-2015-691213-EXCHANGE-Risk grand (Experimental and Computational Hybrid Assessment of NG Pipelines Exposed to Seismic Hazard, www.exchange-risk.eu). This support is gratefully acknowledged.

REFERENCES

[1] O'Rourke M.J. and Liu X., *Response of buried pipelines subjected to earthquake effects*. University of Buffalo, USA, 1999.

[2] Yun H. and Kyriakides S., "On the beam and shell modes of buckling of buried pipelines", *Soil Dynamics and Earthquake Engineering*, 9,179-193, 1990.

[3] ABAQUS (2012). *ABAQUS: theory and analysis user's manual version 6.12*. Providence, RI, USA: Dassault Systemes Simulia.

[4] Timoshenko S.P. and Gere J.M. *Theory of elastic stability*. McGraw-Hill, 1961.

[5] Psyrras N. and Sextos A., "Safety of buried steel natural gas pipelines under earthquake-induced ground shaking: A review", *Soil Dynamics and Earthquake Engineering*, 106, 254-277, 2018.

[6] Vazouras P., Dakoulas P. and Karamanos S.A., "Pipe-soil interaction and pipeline performance under strike-slip fault movements", *Soil Dynamics and Earthquake Engineering*, 72, 48-65, 2015.

[7] Kyriakides S. and Corona E., *Plastic buckling and collapse under axial compression. Mech. Offshore pipelines buckling collapse*, 1, 280-318, Elsevier Science, New York, 2007.

[8] Paquette J.A. and Kyriakides S., "Plastic buckling of tubes under axial compression and internal pressure", *International Journal of Mechanical Sciences*, 48, 855-867, 2006.